15th CIRP Conference on Modelling of Machining Operations

Modeling and Simulation of Machining-Induced Surface Integrity Characteristics of *NiTi* Alloy

Y. Kaynak[a]*, S. Manchiraju[b], I.S. Jawahir[c]

[a]*Department of Mechanical Engineering, Faculty of Technology, Marmara University, Goztepe Campus, Kadikoy, 34722, Istanbul, Turkey*

[b]*Scientific Forming Technology Corporation, Columbus, OH 43235., USA*

[c]*Institute for Sustainable Manufacturing (ISM) and Department of Mechanical Engineering, University of Kentucky, Lexington, KY 40506, USA*

* Corresponding author. Tel.: +90-216-336-5770; fax:+90-216-337-8980.*E-mail address:* yusuf.kaynak@marmara.edu.tr, yusuf_kaynak@yahoo.com

Abstract

NiTi shape memory alloys have gained increased interest in various industries, including biomedical and aerospace applications due to their unique properties such as shape memory effect and superelasticity. Martensitic phase transformation in *NiTi* significantly affects the surface integrity characteristics. This phase transformation needs to be better understood to control and enhance the shape memory and microstructural properties of *NiTi* shape memory alloys. This study presents results of combined experimentation and simulation of cutting-induced phase transformation in orthogonal machining of *NiTi* shape memory alloys. A phenomenological modeling approach was utilized to model machining-induced phase transformation. *NiTi* shape memory alloys alloy were in austenite phases at room temperature. The transformation during dry machining process from austenite to martensite phases, and the resulting volume fraction was successfully simulated using DEFORM 2-D software by implementing a user-defined subroutine. The developed model is capable of capturing the trend of variations in volume fracture and the depth of transformed layer as a function of cutting speed.

1. Introduction

NiTi shape memory alloys (SMAs) have been widely used in various industries for components in aerospace, automotive, biomedical, oil exploration applications [1], seismic isolation, and in composite structures for controlling the vibration [2]. New biomaterials are being continuously developed to respond to the need for better mechanical properties and biocompatibility [3]. Since *NiTi* SMAs combine the shape memory effect, superelasticity and other excellent mechanical properties [3], they have great potential for biomedical [4, 5] and aerospace applications [6, 7].

However, the machining characteristics of SMAs, particularly the effects of machining process on the shape memory behavior and surface integrity characteristics needs to be systematically investigated to establish relationships between the machining process parameters and their shape memory properties, namely to determine the process-microstructure-property relationships [8].

Machining performance of *NiTi* shape memory alloys have been systematically investigated by researchers [9-11], however, only a few researchers have focused on the machining-induced surface integrity of *NiTi* shape memory alloys. Weinert et al. [12] presented the effects of drilling parameters on the microhardness of the subsurface of work material. Kaynak et al. [13] investigated the effects of flood cooling and dry machining on the hardness of the machined surface of $Ni_{49.9}Ti_{50.1}$ alloy. Guo et al. [14] investigated the surface integrity properties of $Ni_{50.8} Ti_{49.2}$ in milling process (with general purpose synthetic coolant) as functions of feed rate and cutting speed, where machined surface hardness was found to be much lower than that of the subsurface. Kaynak et al. [15] investigated the effects of cryogenic machining on the surface integrity characteristics (e.g., surface roughness and

microhardness) of Ni$_{49.9}$Ti$_{50.1}$ alloys. Recently presented extensive experimental studies illustrate that microstructural and shape memory properties of *NiTi* alloys have been substantially affected from cutting parameters and cutting conditions [8, 16].

Deformation mechanism of *NiTi* alloy includes both, the plasticity and martensitic phase transformation during the machining process. Due to the unique thermo-mechanical and shape memory properties, *NiTi* alloys have very sophisticated deformation mechanism depending on critical factors such as deformation temperature, stress state, composition of material, and deformation rate, etc. On the other hand, machining process is inherently a very complex deformation process due to very high strain-rate, temperature, and large strain. Therefore, the modeling and simulation of machining-induced phase transformation is a significant challenge [17]. In fact, only a few studies are found in the literature focusing on the machining-induced phase transformation response of materials. Ramesh and Melkote [18] studied the influence of stress and temperature on the phase transformation temperature of *AISI* 52100 steel in machining process. In their model, they assumed that the phase transformation temperature under certain cutting conditions changes to become a function of hydrostatic and effective stress. Michna et al. [19] made an attempt to simulate the machining-induced phase transformation by utilizing the modified Avrami model. They predicted the deformed layer and compared it with the experiment results.

This study presents prediction of cutting-induced phase transformation in machining of *NiTi* shape memory alloys, and comparison with experimental results.

2. Constitutive Model Used for Phase Transformation and Materials Properties

Shape memory alloys have martensitic phase transformation that significantly influences the deformation mechanism. Since the phase transformation is mainly stress and temperature-dependent, and the machining process depends on both plastic deformation and transformation-induced deformation, this should be taken into account to define the thermo-mechanical response of the shape memory alloys. As the selected *NiTi* alloy was in austenite state at room temperature, the flow stress of the material under high strain-rate, used in this study, was taken from the work by Adharapurapu et al. [20], and austenite plasticity was considered in the process.

While shape memory materials exhibit almost no rate-dependence, using the rate-dependent transformation law can help in regularizing the transformation law and convergence [21]. Anand and Gurtin [21] expressed the rate of change of the volume fraction of martensite, $\dot{v}_M$, in terms of the driving force for transformation f_M and a critical value f_c as

$$\dot{v_M} = \begin{cases} \dot{v_{M0}} \left| \frac{f_M}{f_c} \right|^{\frac{1}{m}} ; f_M > 0 \text{ and } v_M < 1 \\ -\dot{v_{M0}} \left| \frac{f_M}{f_c} \right|^{\frac{1}{m}} ; f_M < 0 \text{ and } v_M > 0 \end{cases} \tag{1}$$

where $\dot{v_{M0}}$ denotes reference transformation rate, m denotes rate exponent. A very small rate exponent, $m = 0.02$, is used to reach almost rate-independent transformation so that the phase transformation will occur only when the driving force f_M is close to the critical value f_c [21]. When the total martensite volume fraction v_M reaches 1, forward transformation ($A \rightarrow M$) is considered complete. The reverse transformation ($M \rightarrow A$) stops when $v_M = 0$. A reference transformation rate of $\dot{v_{M0}}$ is taken as 0.001.

The driving force f_M is defined as the work conjugate to the volume fraction v_M of martensite at a material point; therefore, to implement this, the Helmholtz free energy per unit reference volume is defined [22]. The driving force to increase the volume fraction v_M is derived following Manchiraju and Anderson [22] as;

$$f_t(v_M, \Sigma, T) = \Sigma - \frac{\lambda_T}{T_{eq}} (T - T_{eq}) - hv_M \tag{2}$$

where Σ is the effective stress at the material point. The second term is the force due to chemical free energy associated with the phase transformation [22]. The chemical free energy is constructed to vary linearly with temperature, T, where the equilibrium transformation temperature, T_{eq} is;

$$T_{eq} = \frac{M_s + A_s}{2} \tag{3}$$

M_s and A_s are martensite start and austenite start temperatures, respectively. λ_T is the latent heat per unit reference volume. The third term is the force due to elastic interaction energy, hv_M, between martensite plates, which is assumed to vary quadratically with martensite volume fraction. Volume fraction was represented in the third term as v_M. The transformation strain developed due to martensite volume fraction v_M is given by [23]:

$$\dot{\varepsilon}_{ij}^{Tp} = \frac{3}{2} K_{IJ} h\left(\xi_J\right) \dot{v_M} s_{ij} \tag{4}$$

where: $\dot{\varepsilon}_{ij}^{Tp}$ denotes transformation plasticity strain tensor, K_{IJ} denotes transformation plasticity coefficient from phase one phase to other, $\dot{v_M}$ denotes volume fraction rate, and s_{ij} is deviatoric stress tensor.

The constitutive model was implemented by a user subroutine written in Fortran, and linked to licensed DEFORM 2-D commercially available software.

Machining process of *Ni*-rich shape memory alloy is simulated using the constitutive model just reported. Tests were conducted to obtain those critical parameters of this particular alloy, which were used to calibrate the model by considering uniaxial compression test and a reference stress-strain response, which was experimentally obtained. Material parameters in the model calibrated for *NiTi* alloy include phase transformation, elastic and thermal parameters. Elastic and thermal parameters are given in Table 1.

Phase transformation parameters were: $T_{eq}, \lambda_T, f_c, h,$ Equilibrium transformation temperature, T_{eq}, was found with DSC test as 262.15 °K. Latent heat of transformation per unit volume, λ_T, critical energy barrier for transformation, f_c, and

transformation hardening value, *h,* were 140 MJ/m³, 266 MJ/m³, 250 MPa, respectively, to fit the model to the experimental result.

Table 1. Elastic and thermal properties of work material [24].

	NiTi (Austenite)	*NiTi* (Martensite)
Young Modulus (GPa)	75	41
Poission rate (-)	0.3	0.3
Thermal conductivity (W/m.K)	18	8.6
Thermal expansion coefficients	11x10⁻⁶	6.6x10⁻⁶
Heat capacity (J/g.°C)	0.837	0.320
Emissivity (-)	0.4	0.4

3. Numerical Simulation Procedure

DEFORM 2D commercially available software was used to simulate the orthogonal cutting process of *NiTi* alloy. The created tool and its dimensional properties used in the simulation were determined considering the tool used in the experimental work. Rake angle of cutting tool was - 6° and clearance angle was 6°. The edge radius was set as 25 micrometer, all matching well with the experimental conditions. Mesh, dimension and boundary conditions are given in Fig. 1. Considering the cutting process, workpiece top and right side were allowed to change the heat with environment. The cutting tool's rake angle side and clearance side were allowed to change the heat with the environment. All other sides of work material and cutting tool as shown in Fig. 1 were assumed to have room temperature, T_0.
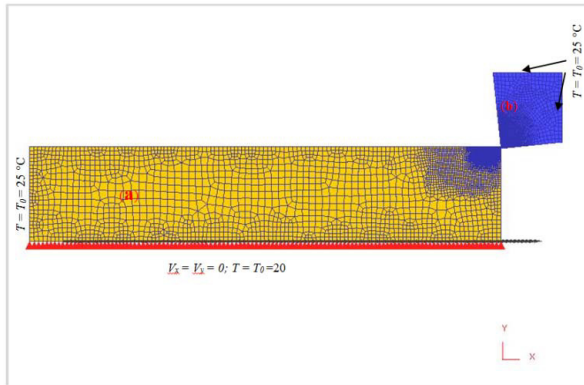

Fig.1. Mesh, dimensions and boundary conditions for (a) work material, and (b) cutting tool.

The cutting tool was selected as a rigid material with a mesh containing 3085 elements. The cutting tool used in orthogonal cutting was uncoated carbide, and it did not have any groove on the rake face. For thermo-mechanical properties of the selected cutting tool, Özel and Zeren's study [25] was utilized as a reference. The given detail of thermo-mechanical properties of cutting tool are: thermal expansion, 4.7 µm/m°C; density 15 g/cm³, poisson rate 0.2, specific heat 203 J/kg/°C, thermal conductivity 46 W/m°C, and young's modulus 800 GPa. Work material, *NiTi* shape memory alloy, was selected as a rigid plastic material with a mesh containing

6100 elements. The flow stress of the material under high strain-rate, used in this study, was taken from the work by Adharapurapu et al. [20], as shown in Fig. 2.
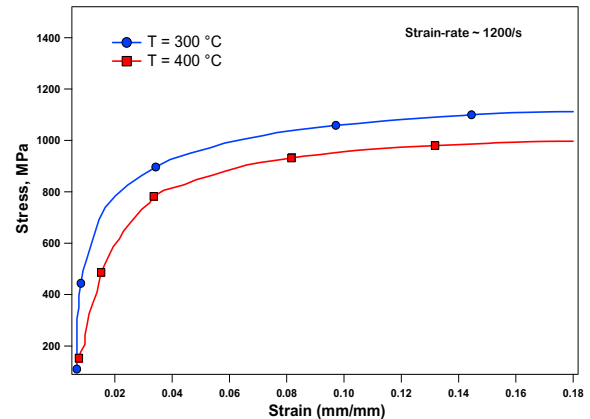

Fig. 2. Dynamic (1200/s) tensile stress-strain curves for annealed *Ti-50.8 Ni* rod at elevated temperatures [20].

Indeed, the ideal model for the simulation conditions was the elasto-plastic one. Neglecting the elastic region of the material's response limits possible output from the simulation of the retained volume fraction. In order to simulate the retained phase, the elasto-plastic model definitely needs to be used; however, the model was not taken into account due to difficulties with the converging issue during the simulation. Ongoing work on this modeling study aims to use elasto-plastic model to predict retained transformation on the machined specimens.

The frictional relation between the cutting tool and the work material was defined by using shear friction model,

$$\tau = m.K_{chip} \tag{5}$$

where τ is stress between rake face of cutting tool and chip; m is the shear factor and K_{chip} is the shear strength of chip material adjacent to the tool-chip interface [26]. Shear factor was taken as 0.7 for all cutting simulations [27]. It should be noted that obtained cutting forces using the given shear factor and experimentally measured force for selected conditions showed acceptable agreement. Since cutting forces are beyond the scope of this paper, they are not presented in this study.

The Cockroft and Latham`s fracture criterion [28], given below, was used.

$$\int_0^{\bar{\varepsilon}} \sigma_1 d\bar{\varepsilon} = D \tag{6}$$

where $\bar{\varepsilon}$ is the effective strain, σ_1 is the maximum principal stress and *D* is a material constant. The critical damage value was computed for each element for each time step and initiated a crack when this value was reached [29]. *D* value was taken as 200. Heat transfer coefficient, *h*, was calibrated using experimental data and taken as 180 KW/m²K. It was assumed that the heat transfer coefficient did not change with velocity; therefore, it was kept constant for all the simulations.

4. Experimental Procedure

The work material used in this study was a binary *NiTi* (*Ni-55.82, Ti-*balance (wt.%)) alloy in the form of cylindrical discs of 94 mm diameter and 3 mm thickness, obtained in a hot rolled condition. The *NiTi* alloy was fully austenitic at room temperature.
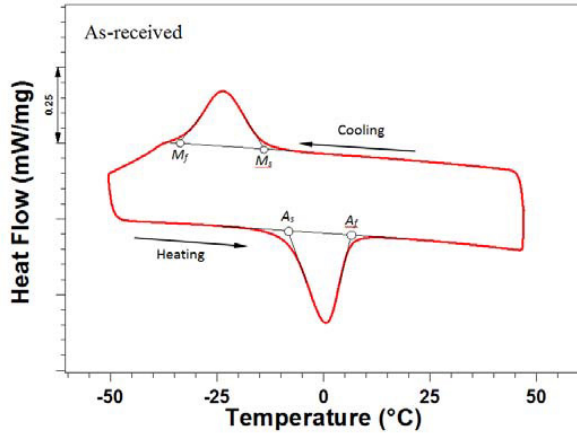

Fig. 3. DSC response of *NiTi* alloy.

This was confirmed by differential scanning calorimetry, where the martensite start, martensite finish, austenite start, and austenite finish temperatures are -14, -34, -8 and 6 ± 1 °C, respectively, for the as-received material (Fig. 3). Dry cutting was performed on the as-received material at room temperature. The actual machining experiments were carried out on a Mazak CNC lathe. Experimental setup is presented in Fig. 4. The cutting tools used in this set of experiments were Kennametal TPGN 220412 (TPG433) grade K313. The edge radius of the tools varied between 22-26 μm. Cutting speeds were 6.25, 12.5 m/min and uncut chip thickness was 0.05 mm.
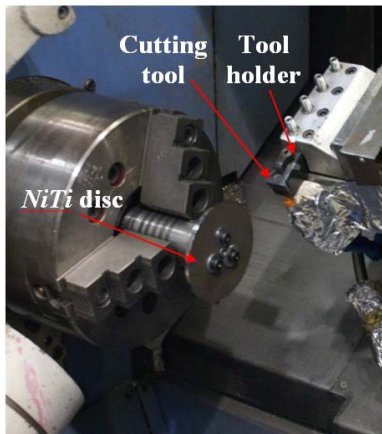

Fig. 4. Experimental setup.

To examine the machined surface- and subsurface-affected layer after the machining processes, specimens were cold-mounted in cross-section, ground and polished using conventional techniques, and etched using a solution of 3.2 vol % *HF* + 14.6 vol. % *HNO₃* + 82.2 vol. % *H₂O*. The microstructure of these specimens was examined by digital optical microscopy and the depths of the affected layers were determined. To calibrate variables used in the model, compression tests have been carried out. The compression tests were conducted on a 100 kN capable Landmark MTS servohydraulic test frame using a constant strain-rate of 10^{-4} mm s^{-1}.

5. FEM Simulation Results

The main focus of this section is to assess whether or not the presented model is capable of capturing the trend of cutting-induced phase transformation and the depth of affected layer. Therefore, the main output evaluated and analyzed was the machining-induced martensitic volume fraction and the effect of cutting speed on phase transformation in the cutting process of *NiTi* alloy. Since the temperature and its variations play a substantial role on determining the driving force for phase transformation,
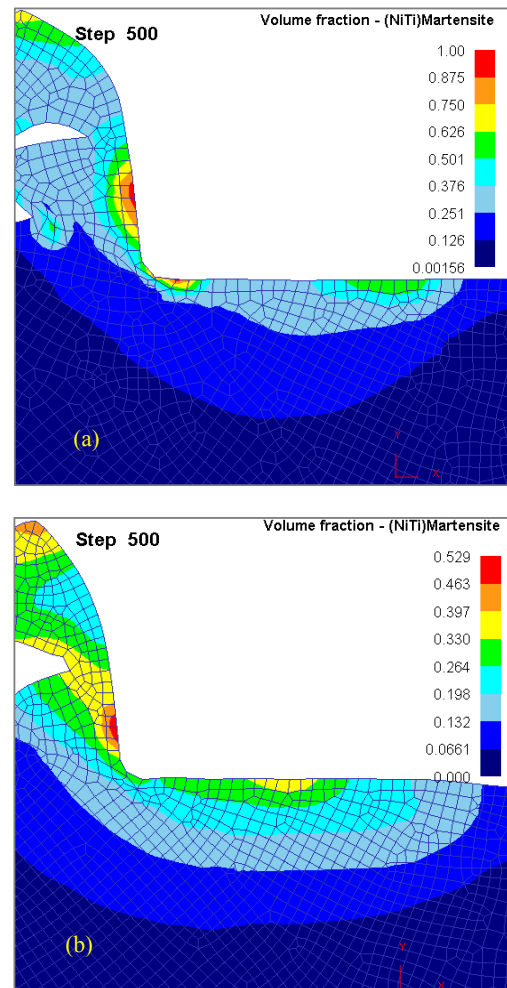

Fig. 5. Prediction of martensitic volume fraction resulting from the cutting process of *NiTi* alloy at (a) 6.25 m/min (b) 12.5 m/min cutting speed.

the temperature change needs to be considered. To predict the effects of temperature on phase transformation, two different cutting speeds are considered.

It is a well-known fact that increased cutting speed leads to rising temperature. Fig. 5 shows predicted martensitic volume fraction results of *NiTi* alloy under two different cutting speeds, namely Fig. 5 (a) presents the obtained results at lower cutting speed ($V = 6.25$ m/min), while Fig. 5(b) presents the obtained results at higher cutting speed ($V = 12.5$ m/min). It is obvious that under selected cutting conditions (dry cutting) and parameters, phase transformation takes place on the newly generated chips, surface of machined workpiece and beneath the machined surface.

Another finding from simulation results is that higher martensitic volume fraction takes place at the machined surface and side of chip contact with the rake face of cutting tool. This is the results of effective stress distribution and temperature. The most notable finding is that as cutting speed increases, the martensite volume fraction decreases, which can be evidently seen in Figure 5. It should be kept in mind that although these predictions show transformation during the cutting process that will be different to the retained transformation, but the trend will not change.

6. Experimental Results and Validation of the FE Model

Fig. 6 shows the cross-sections of the specimens machined at cutting speeds of 6.25 and 12.5 m/min under dry conditions. Extensive twinning within the grains was observed on the surface and subsurface of the machined samples [8].

Under optical microscopy, these twins look like polishing marks on the surface and subsurface, as shown in Fig. 6. The depth of the affected layer (*h*) can be determined by using the observed extensive twinning within the grains on the surface and subsurface as a measure of machining-induced layer. It is evident that the depth of the affected layer is much higher in the machined specimen at lower cutting speed ($V = 6.25$ m/min) in comparison with the machined specimen at lower cutting speed ($V = 12.5$ m/min). The depth of affected layer is approximately 180 ±20 µm and 140 ±20 µm at 6.25 and 12.5 m/min cutting speeds, respectively. Increased cutting speed reduces the depth of affected layer indicating that the depth of transformation is much higher at lower cutting speed ($V = 6.25$ m/min).

Although two different cutting speeds are presented in this study, more details of the experimental work was presented elsewhere and was reported that as cutting speed increases, the depth of affected layer continues to decrease until 50 m/min cutting speed [8].

As it is presented in previous section, at lower cutting speeds, martensitic volume fraction at some region, particularly around the edge of cutting tool, was found indicating that complete transformation from austenite to martensite took place. However, at higher cutting speed ($V = 12.5$ m/min), the transformation rate at same region is around 0.5 indicating that partial transformation took place. Experimental findings support this relation. Experimentally observed cross section of machined specimens illustrate that

on the surface and just below the surface, more twins are observed at lower cutting speed, compared with the higher cutting speed condition. Besides, larger affected depth at lower cutting speed is a good indicator to support the relation between cutting temperature and transformation in machining of *NiTi* alloy.
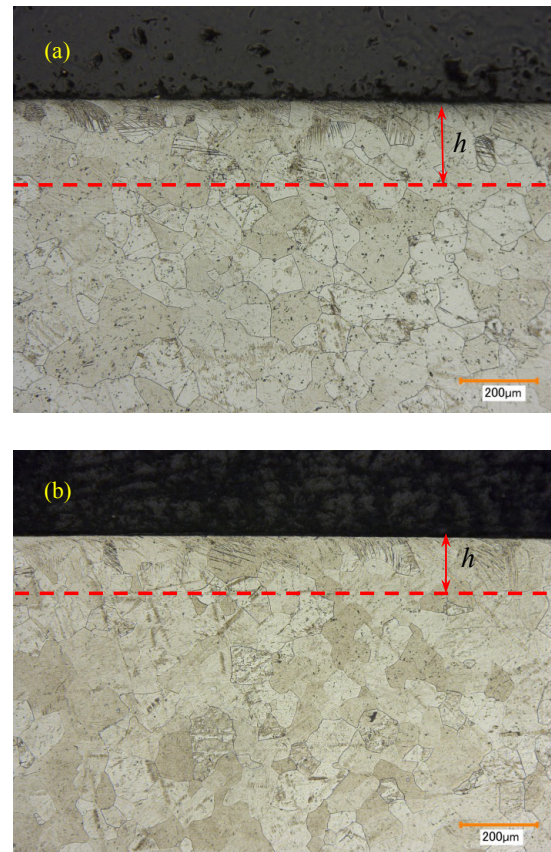

Fig. 6. Experimental results: Cross-sectional microstructure of *NiTi* alloy machined at (a) 6.25 and (b) 12.5 m/min cutting speeds [8].

Phase transformation as one of the significant surface integrity characteristics can take place during machining of various materials depending on cutting conditions, parameters, and work material's properties. In order to control the effects of phase transformation on the thermal, mechanical and superelasticity properties of the finished products, it is essential to be able to predict transformation for various cutting conditions and machining parameters. This study presents an effort to predict machining-induced phase transformation, but much more effort is needed to enhance the predictive capability of this model for better and quantitative predictions.

7. Conclusions

A phenomenological model was developed to simulate machining process of *NiTi* shape memory alloys and predict machining-induced phase transformation response of this

alloy. Two different cutting speeds were considered for simulating dry machining of *NiTi* alloy. The obtained simulation results were validated with experimental study. This study shows that the model is capable of capturing the trend of transformation induced by the machining process and the cutting speed. For the given conditions, it was found that martensitic volume fraction is much larger at the machined surface as compared to the subsurface of machined *NiTi* alloy. It is important to note that increased cutting temperature leads to reduced martensitic volume fraction in machining of *NiTi* shape memory alloys. Ongoing study focuses on enhancing material properties calibration to improve the predictive capability of the model for much accurate predictions. Ongoing study also includes simulating forward and reverse transformation and predicating the resulting volume fraction and depth of transformation.

Acknowledgements

References

[1] Lagoudas, D.C., Shape Memory Alloys: Modeling and Engineering Applications. New York, Springer., 2008.

[2] Han, Y.L., Li, Q.S., Ai-Qun, L., Leung, A.Y.T., Lin, P.H., Structural vibration control by shape memory alloy damper. Earthquake Engineering & Structural Dynamics, 2003. 32(3): p. 483-494.

[3] Fadlallah, S.A., Bagoury, N., Gad El-Rab, S., Ahmed, R.A., El-Ousamii, G., An overview of NiTi shape memory alloy: Corrosion resistance and antibacterial inhibition for dental application. Journal of Alloys and Compounds, 2014. 583: p. 455-464.

[4] Rondelli, G., Corrosion resistance tests on NiTi shape memory alloy. Biomaterials, 1996. 17(20): p. 2003-2008.

[5] Shabalovskaya, S.A., On the nature of the biocompatibility and on medical applications of NiTi shape memory and superelastic alloys. Bio-medical materials and engineering, 1996. 6(4): p. 267-289.

[6] Hartl, D.J. and D.C. Lagoudas, Aerospace applications of shape memory alloys. Proceedings of the Institution of Mechanical Engineers Part G-Journal of Aerospace Engineering, 2007. 221(G4): p. 535-552.

[7] Calkins, F.T. and J.H. Mabe, Shape Memory Alloy Based Morphing Aerostructures. Journal of Mechanical Design, 2010. 132(11):111012-19.

[8] Kaynak, Y., Karaca, H.E., and Jawahir, I.S., Cutting Speed Dependent Microstructure and Transformation Behavior of NiTi Alloy in Dry and Cryogenic Machining. Journal of Materials Engineering and Performance, 2015. 10.1007/s11665-014-1247-6.

[9] Kaynak, Y., Karaca, H.E., Noebe, R.D., Jawahir, I.S., Tool-wear analysis in cryogenic machining of NiTi shape memory alloys: A comparison of tool-wear performance with dry and MQL machining. Wear, 2013. 306(1-2): p. 51-63.

[10] Kaynak, Y., Robertson, S., Karaca, H.E., Jawahir I.S., Progressive tool-wear in machining of room-temperature Austenitic NiTi Alloys: The influence of cooling/lubricating, melting, and heat treatment conditions. Journal of Materials Processing Technology, 2015. 215: p. 95-104.

[11] Weinert, K. and Petzoldt, V., Machining of NiTi based shape memory alloys. Materials Science and Engineering A, 2004. 378(1-2): p. 180-184.

[12] Weinert, K.,Petzoldt, V., and D. Kotter, Turning and drilling of NiTi shape memory alloys. CIRP Annals-Manufacturing Technology, 2004. 53(1): p. 65-68.

[13] Kaynak, Y., Karaca, H.E., and Jawahir, I.S., Sustainability evaluation in machining of NiTi shape memory alloy. 1st international Conference on Sustainable Life in Manufacturing (SLIM 2010), 2010: p. 40-47.

[14] Guo, Y., Klink, A., Fu, C., Snyder, J., Machinability and surface integrity of Nitinol shape memory alloy. CIRP Annals-Manufacturing Technology, 2013. 62(1): p. 83-86.

[15] Kaynak, Y., Karaca, H.E., and Jawahir, I.S., Cryogenic machining of NiTi shape memory alloy. 6th Int. Conference and Exhibition on Design and Production of Machines and Dies/Molds, 2011: p. 23-26.

[16] Kaynak, Y., Tobe, H., Noebe, R.D., Karaca, H.E., Jawahir, I.S., The effects of machining on microstructure and transformation behavior of NiTi alloy. Scripta Materialia, 2014. 74: p. 60-63.

[17] Kaynak, Y., Process-induced surface integrity in machining of NiTi shape memory alloys University of Kentucky, 2013. PhD Dissertation.

[18] Ramesh, A. and Melkote, S.N.,Modeling of white layer formation under thermally dominant conditions in orthogonal machining of hardened AISI 52100 steel. International Journal of Machine Tools & Manufacture, 2008. 48(3-4): p. 402-414.

[19] Schulze, V., Michna, J., Zanger, F., Pabst, R., Modeling the process-induced modifications of the microstructure of work piece surface zones in cutting processes. Advanced Materials Research, 2011. 223: p. 371-380.

[20] Adharapurapu, R.R., Jiang, F., Bingert, J.F., Vecchio, K.S., Influence of cold work and texture on the high-strain-rate response of Nitinol. Materials Science and Engineering: A, 2010. 527(20): p. 5255-5267.

[21] Anand, L., Gurtin, M.E., 2003. Thermal effects in the superelasticity of crystalline shape-memory materials. Journal of the Mechanics and Physics of Solids 51, 1015-1058.

[22] Manchiraju, S. and Anderson, P., Coupling between martensitic phase transformations and plasticity: A microstructure-based finite element model. International Journal of Plasticity, 2010. 26(10): p. 1508-1526.

[23] Deform, U.M., Deform 2D user manual. 2013: p. 120-121.

[24] Shaw, J.A., 2000. Simulations of localized thermo-mechanical behavior in a NiTi shape memory alloy. International journal of plasticity 16, 541-562.

[25] Özel, T. and E. Zeren, Finite element modeling the influence of edge roundness on the stress and temperature fields induced by high-speed machining. The International Journal of Advanced Manufacturing Technology, 2007. 35(3-4): p. 255-267.

[26] Yen, Y.-C., Jain, A., Chigurupati, P., Wu, W., Altan, T., Computer simulation of orthogonal cutting using a tool with multiple coatings. Machining science and technology, 2004. 8(2):305-326.

[27] Shao, F., Liu, Z., Wan, Y., Shi, Z., Finite element simulation of machining of Ti-6Al-4V alloy with thermodynamical constitutive equation. The International Journal of Advanced Manufacturing Technology, 2010. 49(5-8): p. 431-439.

[28] Cockcroft, M. and D. Latham, Ductility and the workability of metals. J Inst. Metals, 1968. 96(1): p. 33-39.

[29] Vijay Sekar, K. and M. Pradeep Kumar, Finite element simulations of Ti6Al4V titanium alloy machining to assess material model parameters of the Johnson-Cook constitutive equation. Journal of the Brazilian Society of Mechanical Sciences and Engineering, 2011. 33(2): p. 203-211.